Birefringence Induced in Optical Rib Waveguides by Thermal and Mechanical Stresses

Giuseppe Grasso, Francesco De Leonardis and Vittorio M. N. Passaro
Photonics Research Group, Dipartimento di Ingegneria Elettrica e dell'Informazione, Politecnico di Bari, via Edoardo Orabona n. 4, 70125 Bari, Italy
Tel. +39 0805963850, URL: http://dee.poliba.it/photonicsgroup
E-mail: vittorio.passaro@poliba.it

Abstract:
In this paper a multiphysics approach to study the optical properties of integrated waveguides influenced by thermal and mechanical stress is presented. The heating and pressure effects are evaluated by means the Heat Transfer and Structural Mechanics modules respectively. Finally, the Electromagnetics Module is used in order to evaluate the optical eigenfunctions and eigenvalues.

Keywords: Integrated Optics, Silicon Photonics, Birefringence, Multiphysics Modeling.

1. Introduction

For decades, silicon has been considered the optimal material for electronics mass production. In the last few years, the possibility to realize highly performing active and passive photonic integrated devices using Silicon-on-Insulator (SOI) technological platform has been widely proved [1]. One of the most important aspects of any integrated optical technology for sensing or communication applications is the evaluation and control of the optical birefringence [2]-[6].
Generally speaking, the optical birefringence depends on the waveguide cross section, material and plasma dispersion effect [7], and mechanical stress. In this contest, a detailed study has been proposed in [8], demonstrating that the stress engineering can be considered as an effective tool to modify or eliminate polarization dispersion in SOI waveguide devices, for a wide range of waveguide cross-section shapes and sizes. In addition, calculations and experiments proposed in [8] confirm that the SiO_2 cladding induced-stress can be used to eliminate the birefringence in SOI waveguides of arbitrary shapes for typical film stress values ranging from 100 to 300 MPa. Therefore, the goal of this work is to develop a self-consistent and integrated approach, in order to generalise the analysis presented in [8] including thermal and mechanical stress effects on guided-wave propagation in optical rib waveguides.
In practical applications, a rib waveguide is often in contact with a surface at higher temperature that causes heat flow into the device: this results in material strain and, ultimately, in an optical birefringence. Besides, in many applications of such components, strain is also produced by a pressure that acts on the device. The situation is illustrated in Fig. 1 (a), where F is the force applied on the device and Q is the heat propagating into it. A silicon-on-insulator rib waveguide is in contact with an aluminum layer through a silica layer; the heat flow is caused by the heated aluminum layer whose temperature is higher than that of the rib. The aluminum layer also transmits the pressure on the component. The stresses applied to the waveguide material structure cause each mode to be rotated. Thus, in this paper we use Comsol Multiphysics™ [9] to obtain a fully integrated simulations of SOI waveguides in order to estimate the birefringence effect.

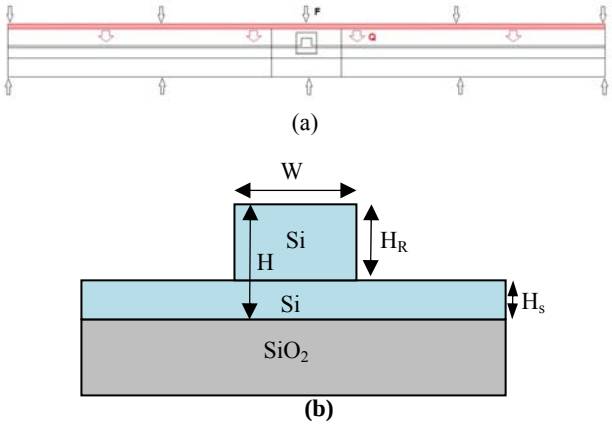

Figure 1. (a) Domain structure; (b) SOI waveguide cross-section.

2. Physical Modeling

The goal of this section is to analyze the thermal and stress influence on the guiding properties of SOI waveguides. In this context, it is worth to briefly describe the procedure for the effective refractive index calculations for both quasi-TE and quasi-TM modes. With the aim to realize self-consistent simulations, we have implemented an integrated algorithmic procedure based on Finite Element Method (FEM) [9], in which the FEM electromagnetic module works together with

the FEM heat transfer and stress modules in order to take into account the thermal and stress effects on the material refractive index.

At the first step, the thermal distribution into the structure is evaluated considering the heat propagation from the aluminum layer towards the SOI waveguide, as described by the following partial differential equation:

$$\rho C \frac{\partial T}{\partial t} + \nabla \cdot \left(-k \nabla T\right) = Q \qquad (1)$$

being T the temperature variable, ρ the density, C the heat capacity, k thermal conductivity, and Q the heat source (or sink).

Thus, the solution of Eq. (l) is obtained by setting the temperature boundary condition at the interface between the aluminum layer and the adjacent layer. Fig. 2 shows the temperature distribution in all active domains and in steady-state regime, assuming the aluminum and room temperature $T_{Al} = 350\ K$ and $T_{room} = 293\ K$, respectively. Hereinafter, the simulations are performed considering a mesh with 76776 degrees of freedom.

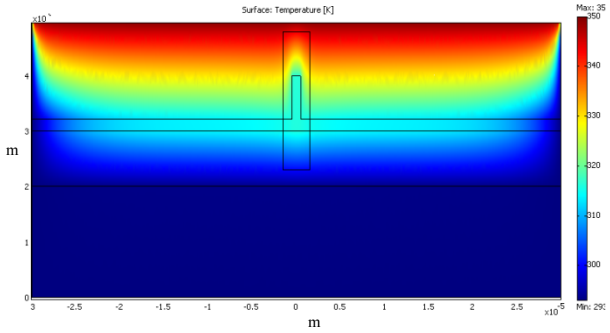

Figure 2. Steady-state temperature distribution induced by aluminum layer at $T_{Al} = 350\ K$.

The plot clearly evidences that, although the temperature distribution changes along the complete structure in the range 350K-293K, the temperature inside the region supporting the optical modes (T_{ridge}) can be considered constant and equal to 315 K for the case simulated by us. In this context, once the temperature value in the vicinity of the waveguide ridge has been evaluated, the induced strain and stress fields inside the optical waveguide can be calculated by solving the following equation [8]:

$$\begin{bmatrix} \sigma_x \\ \sigma_y \\ \sigma_z \end{bmatrix} = \frac{E_Y}{(1+\nu)(1-2\nu)} \begin{bmatrix} 1-\nu & \nu & \nu \\ \nu & 1-\nu & \nu \\ \nu & \nu & 1-\nu \end{bmatrix} \begin{bmatrix} \varepsilon_x \\ \varepsilon_y \\ \varepsilon_z \end{bmatrix} - \frac{\alpha_{thermal} E_Y \left(T_{ridge} - T_{room}\right)}{(1-2\nu)} \qquad (2)$$

where $\sigma_{x,y,z}$ and $\varepsilon_{x,y,z}$ represent the stress and strain components along the x, y and z reference directions, respectively, E_Y is the Young's modulus and ν is the Poisson's ratio. In addition, with the aim to generalize our model, the pressure effect on the device is taken into account by solving Eq. (2) with appropriate boundary condition in the Plane Strain module. In particular, we set the edge load (N/m^2) in the y-direction F_y, at the interface with the metal layer. Hereinafter, the physical parameters listed in Table I are always assumed in the simulations.

Table I. Physical parameters used in simulations.

PARAMETERS	VALUES
Si Young's modulus, E_Y(Si)	170 (GPa)
SiO2 Young's modulus, $E_Y(SiO_2)$	70 (GPa)
Si Poisson's ratio, ν (Si)	0.28
SiO2 Poisson's ratio, ν (SiO_2)	0.17
Si linear thermal expansion coefficient, $\alpha_{thermal}$ (Si) at 293 K	2.6×10^{-6} (K^{-1})
SiO2 linear thermal expansion coefficient, $\alpha_{thermal}$ (SiO_2) at 293 K	0.5×10^{-6} (K^{-1})
Photoelastic coefficient p_{11}(Si)	-0.101
Photoelastic coefficient p_{12}(Si)	0.0094
Photoelastic coefficient $p_{11}(SiO_2)$	0.16
Photoelastic coefficient $p_{12}(SiO_2)$	0.27

Fig. 3 shows the Von Mises stress defined as:

$$2\sigma_e^2 = \left(\sigma_x - \sigma_y\right)^2 + \left(\sigma_y - \sigma_z\right)^2 + \left(\sigma_z - \sigma_x\right)^2$$

The plot represents the distribution $\sigma_e(x,y)$ as induced by a temperature metal layer of $350\ K$ and an applied external pressure $F_y = 10^5\ N/m^2$. As it is evident, the stress field is mainly concentrated in the waveguide region confirming as the thermal and stress effect can strongly influence the optical modes propagating into the device.

The solution of Eq. (2) (see Fig. 3) is then used to evaluate the stress-induced material anisotropy as described by the following relations [8]:

$$\begin{cases} n_x - n_0 = -B_1\sigma_x - B_2\left(\sigma_y + \sigma_z\right) \\ n_y - n_0 = -B_1\sigma_y - B_2\left(\sigma_x + \sigma_z\right) \end{cases} \qquad (3)$$

being n_0 the refractive index of the material without stress (Si or SiO_2), and B_1 and B_2 the stress-optical constants dependent by the material photoelastic tensor (p_{ij}), defined as in [8].

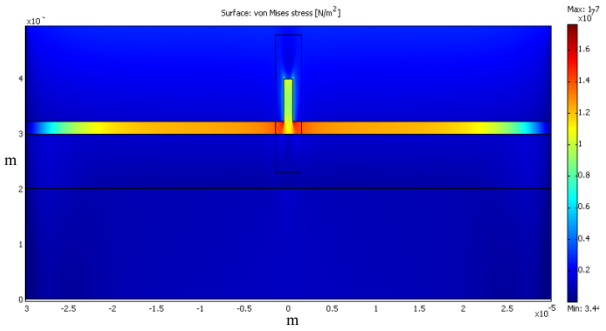

Figure 3. Von Mises stress distribution for T_{Al} = 350 K and $F_y = 10^5$ N/m^2.

Finally, optical mode field distributions propagating within the device and their effective indices *neff* can be calculated as eigenfunctions and eigenvalues of the following equation:

$$\nabla_t \times \left(\varepsilon_{rczz}^{-1} \nabla_t \times \mathbf{H_t}\right) - \tilde{\varepsilon}_{rct} \nabla_t \left(\mu_{rzz}^{-1} \nabla_t \cdot \mu_{rt} \mathbf{H_t}\right) - \left(k_0^2 \mu_{rt} - \beta^2 \tilde{\varepsilon}_{rt}\right) \mathbf{H_t} = 0 \quad (4)$$

where ε_{rczz} , and μ_{rzz} are the z-components of relative permittivity and permeability tensors, respectively. The terms ε_{rct} , and μ_{rt} represents the 2-by-2 tensors in the transversal x-y plane.

It is worth to note that, for accuracy reasons, the calculation window for the stress module is 40 times larger than the window require for the calculation of the waveguide modes.

3. Numerical Results

For the following simulations, we consider two different SOI waveguides, named Wg1 and Wg2, characterized by the following dimensions properly named according to the schematic shown in Fig. 1(b):

- Wg1: H_S = 0.22 μm, W = 1 μm, H = 1 μm, H_R =0.78 μm;
- Wg2: H_S = 0.22 μm, W = 0.5 μm, H = 0.61 μm, H_R =0.39 μm.

For both waveguides considered the first and the second mode are always aligned as a quasi-TE, and a quasi-TM mode, respectively. Figs. 4 and 5 show the dominant component of the electric field for quasi-TE and quasi-TM modes respectively, and assuming T_{Al} = *350 K* and $F_y = 10^5$ *N/m*^{2}.

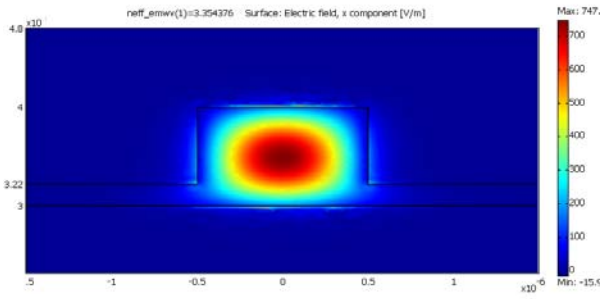

Figure 4. Electric field x-component (quasi-TE mode) for T_{Al} = 350 K and $F_y = 10^5$ N/m^2 , (Wg1).

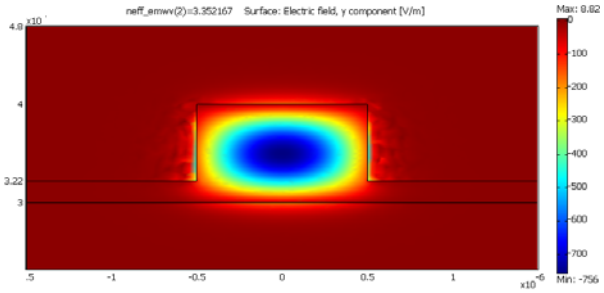

Figure 5. Electric field y-component (quasi-TM mode) for T_{Al} = 350 K and $F_y = 10^5$ N/m^2 , (Wg1).

Performing a number of simulations based on the multiphysics approach described before, we evaluate the thermal and stress dependence of the effective refractive index. The results for the waveguide Wg1 are shown in Figs. 6 and 7, where the effective refractive index is plotted as a temperature and pressure function, respectively. The curves indicate that the effectice refractive index for quasi-TE, and quasi-TM modes increases by increasing the temperature with a thermal slope (S_{th}) of 5.92×10^{-7}, and 4.33×10^{-7} RIU/K, respectively. The opposite trend is observed in the case of pressure changes (see Fig. 7) where a negative pressure slope (S_p) of -2 $\times10^{-12}$, and -5.67×10^{-12} RIU/(N/m^2) are obtained for quasi-TE and quasi-TM modes, respectively.

Similar simulations have been performed for the waveguide Wg2 as shown in Figs. 8 and 9. Our investigations indicate that the Wg2 presents a S_{th} coefficient of about 6.31×10^{-7} and 4.51×10^{-7} RIU/K for quasi-TE, and quasi-TM modes, respectively. On the contrary, observing Fig. 9, the pressure slope S_p assumes values of -2.85×10^{-10}, and -8.23×10^{-11} RIU/(N/m^2) for quasi-TE and quasi-TM modes, respectively.

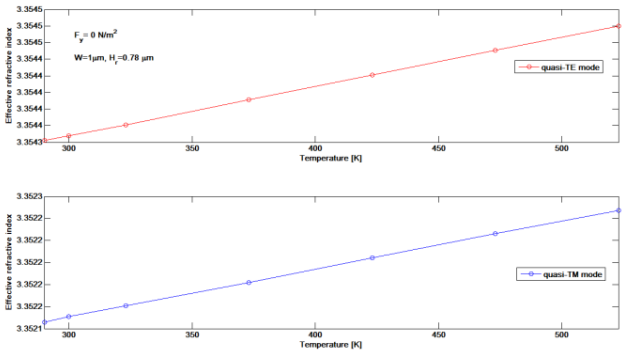

Figure 6. Effective refractive index versus the temperature for quasi-TE and quasi-TM modes (Wg1).

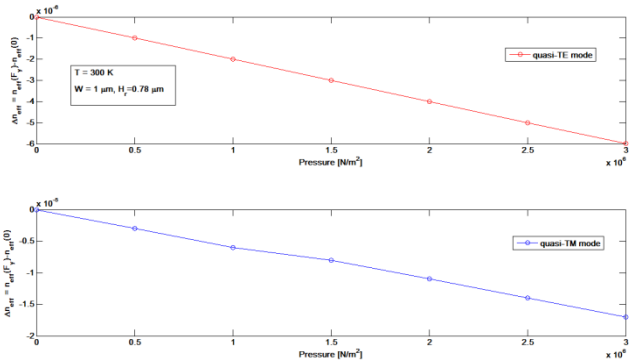

Figure 7. Effective refractive index versus applied pressure for quasi-TE and quasi-TM modes (Wg1).

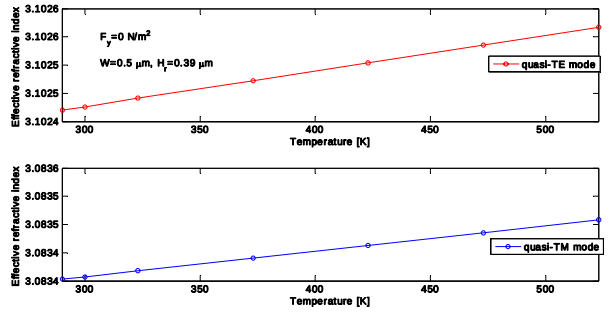

Figure 8. Effective refractive index versus temperature for quasi-TE and quasi-TM modes (Wg2).

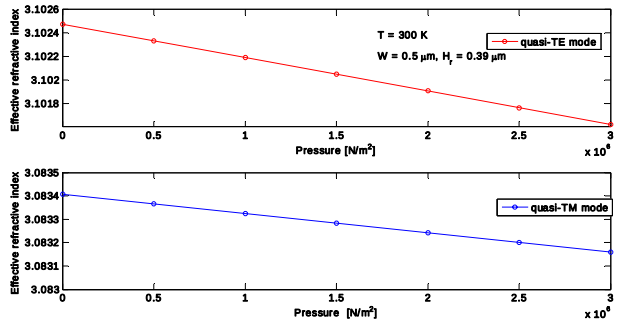

Figure 9. Effective refractive index versus applied pressure for quasi-TE and quasi-TM modes (Wg2).

4. Conclusions

In this paper a fully integrated multiphysics model, involving heat transfer, mechanical stress and electromagnetic modules, has been used for SOI waveguides. Physical effects induced by heating and external pressure acting on the waveguide structure have been investigated. Effective refractive index changes for quasi-TE and quasi-TM optical modes have been calculated for SOI waveguides with micro and nano-scale cross section.

Through this calculation, a thermal and pressure slope has been estimated in order to realize an useful tool for the design of optical waveguides under different temperature and pressure conditions.

5. References

1. V. M. N. Passaro Ed., *Silicon Photonics*.Research Signpost Publ., Kerala, India (2006), ISBN 81-308 0077-2.

2. Z. C. Wang and D. X. Dai, "Ultrasmall Si nanowire-based polarization rotator," J. Opt. Soc. Am. B **25**(5), 747–753 (2008).

3. H. Fukuda, K. Yamada, T. Tsuchizawa, T. Watanabe, H. Shinojima, and S. Itabashi, "Polarization rotator based on silicon wire waveguides," Opt. Express **16**(4), 2628–2635 (2008).

4.D. Dai and J. E. Bowers, "Novel concept for ultracompact polarization splitter-rotator based on silicon nanowires," Opt. Express **19**(11), 10940–10949 (2011).

5. Liu Liu, Yunhong Ding, Kresten Yvind, and Jørn M. Hvam, "Efficient and compact TE–TM polarization converter built on silicon-on-insulator platform with a simple fabrication process," Opt. Lett. **36**, 1059-1061 (2011)

6. B. Troia, F. De Leonardis, M. Lanzafame, Muciaccia, G. Grasso, G. Giannoccaro, C.E. Campanella, V. M. N Passaro, "Design and Optimization of Polarization Splitting and Rotation Devices in Silicon-on-Insulator Technology", *Advances in Optoelectronics*, 490405 (2014).

7. R. A. Soref, B. R. Bennett, Electrooptical Effects in Silicon, *J. Quantum Electronics*, **QE-23**, 123-129 (1987).

8. W. N. Ye, D. X. Xu, S. Janz, P. Chaben, M. J.Picard, B. Lamontagne, N. G. Tarr, "Birefringence Control Using Stress Engineering in Silicon-on-Insulator (SOI) Waveguides", *J. Lightwave Technology*, vol. **23**, n. 3, 1308-1318 (2005).

9. Comsol Multiphysics, ver. 3.2, *single license* (COMSOL Inc., Stockholm, Sweden), 2005.